Nouri *et al. Virology Journal* (2025) 22:345
https://doi.org/10.1186/s12985-025-02949-7

Virology Journal

RESEARCH Open Access

Rapid detection of herpes simplex virus types 1 and 2 using a G-quadruplex aptamer-based biosensor

Sepehr Nouri[1*], Soheil Shajari[1], Hassan Mohabatkar[1*] and Mandana Behbahani[1]

Abstract

Herpes simplex virus types 1 and 2 (HSV-1 and HSV-2), which cause oral and genital herpes in humans, are prevalent worldwide. ELISA, real-time PCR, and cytological assays are conventional methods for detecting these viruses, but they are expensive and time-consuming. The main purpose of this study was to design a specific G-quadruplex aptamer for the simple and rapid detection of HSV-1 and HSV-2. In this study, a specific aptamer was designed using bioinformatics tools for binding to the glycoprotein gD in HSV-1 and HSV-2. After evaluating the binding of the aptamer to gD, based on the stability scores of the secondary and tertiary structures and molecular docking, the aptamer AptNR88 was selected, and its binding to the target protein was confirmed experimentally using a colorimetric system with gold nanoparticles. Gold nanoparticles with an average size of 30 nm were synthesized, and the AptNR88 was coated on them through hydrogen bonds and electrostatic interactions. The concentration of AptNR88 was subsequently optimized for resistance against salt-induced aggregation. The color changes of gold nanoparticles from red to purple due to salt aggregation were observed only in the presence of the AptNR88-virus complex after 15 min. These results confirmed the specific binding of AptNR88 to the gD of HSV-1 and HSV-2. The limit of detection (LOD) for AptNR88 was approximately 11.7 copies/ml for HSV-1 and 15.7 copies/ml for HSV-2. These results indicate that the designed aptamer for detecting these two viruses is sufficiently sensitive and specific.

Keywords Herpes simplex virus, Aptamer, Gold nanoparticles, Bioinformatics tools, Colorimetric assay

Introduction

Herpes simplex viruses are classified under the subfamily Alphaherpesviruses in the family Herpesviridae [1–3]. Herpes simplex virus infection occurs worldwide, and epidemiological studies show increased infection rates in most countries [4, 5]. By 2020, 3.8 billion people under the age of 50 (64%) worldwide were infected with HSV-1, which is the main cause of oral herpes. Additionally, 520 million people aged 15 to 49 years (13%) worldwide are infected with HSV-2, which is the main cause of genital herpes [6].

The genome of herpes simplex virus is a double-stranded DNA, approximately 150 kb, and contains at least 74 open reading frames (ORFs) [7, 8]. HSV-1 and HSV-2 show nearly 70% genomic similarity. These two have similar genomic structures, with sequence homologies reaching 83% similarity in their protein-coding regions [9]. The envelope of HSV, the outer layer of the virion, is generally composed of 10 main glycoproteins

*Correspondence:
Sepehr Nouri
sepehrnouri76@gmail.com
Hassan Mohabatkar
h.mohabatkar@ast.ui.ac.ir

Full list of author information is available at the end of the article

Graphical Abstract

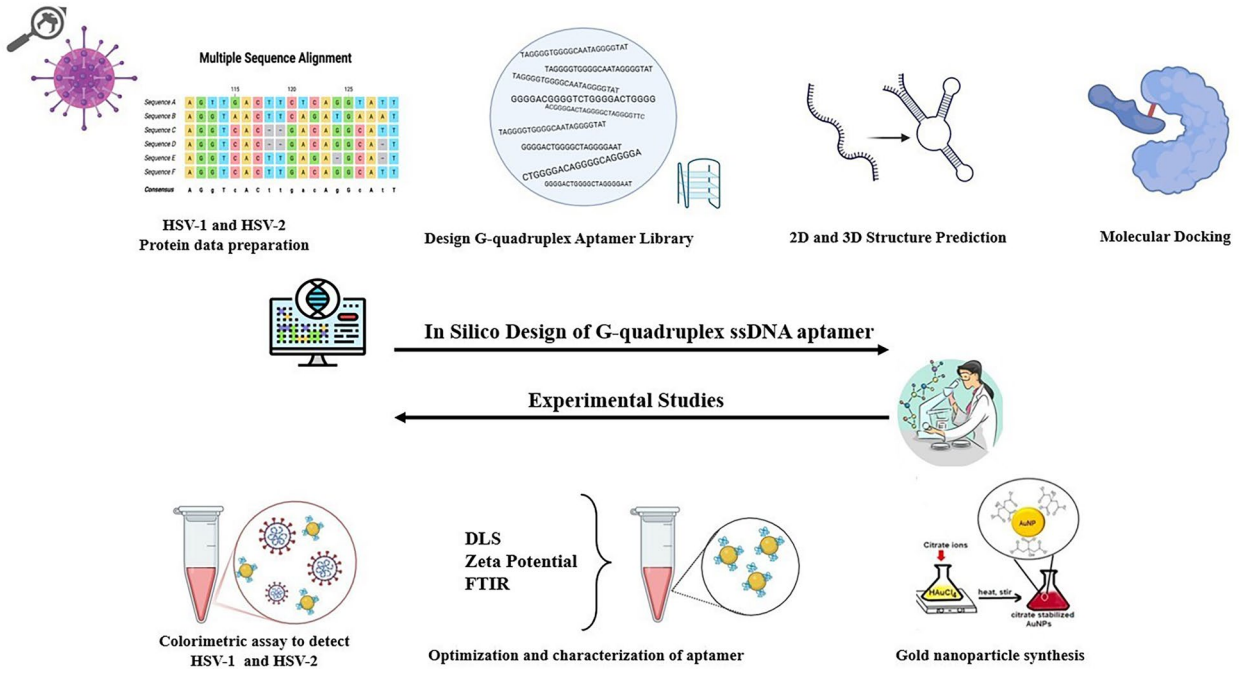

[10–12]. Four glycoproteins (gB, gD, gH, and gL) are essential for viral entry and cell fusion [13]. The glycoprotein gD has a high degree of similarity between the two viruses, HSV-1 and HSV-2. Furthermore, there is an even higher degree of conservation among strains of these viruses, and it has no sequence similarity with other glycoproteins [14, 15]. This protein is an asymmetric homodimer in the viral envelope [16]. Glycoprotein gD is only found in the envelope of HSV-1 and HSV-2, which makes it a strong candidate for detection studies of these viruses [17].

HSV-1 and HSV-2 are often transmitted through skin contact, saliva, sores, or genital contact with an infected individual [18, 19]. Common symptoms include blisters or open sores around the mouth or genital areas [20, 21]. Rarely, HSV-1 infection can lead to more severe complications such as meningoencephalitis or keratitis [22]. Various diagnostic methods such as real-time PCR, ELISA, and rapid diagnostic or cytological assays, have been described to detect HSV-1 and HSV-2. However, in addition to offering higher accuracy, sensitivity, and specificity, aptamer-based detection requires less equipment and costs [23].

Oligonucleotide aptamers are small ssDNA and ssRNA molecules, with a typical length ranging from 25 to 100 nucleotides, that can bind to various molecules such as proteins, carbohydrates, lipids, ions, and small cells. They have unique 3D structures (hairpin, stem-loop, pseudoknot, triplex, and quadruplex) [24]. Oligonucleotide aptamers exhibit several advantages over monoclonal antibodies, such as simple structure, smaller size, non-immunogenicity, high accessibility to chemical modifications, and ease of production and storage [25]. Specifically, G-quadruplex aptamers are a unique class of nucleic acid structures formed by guanine-rich oligonucleotides. Compared with other structures, they show higher stability, improved electrostatic interactions due to their significant charge density, and high accessibility to chemical modifications [26]. Selection of G-quadruplex aptamers can be performed using partially randomized G-rich oligonucleotide libraries combining SELEX with rational design methods [27].

In the reported literature, aptamers designed against HSV have not adopted a G-quadruplex conformation. They have been investigated for therapeutic applications rather than for diagnostic purposes. In this study, a specific G-quadruplex aptamer was designed and optimized using bioinformatics tools to rapidly detect HSV-1 and HSV-2 by binding to glycoprotein gD. After evaluating the stability scores of the secondary and tertiary structures of the aptamers using RNAfold, QGRS mapper, and Rosetta FARFAR servers, molecular docking was performed with HDOCK and HADDOCK servers, and the aptamer-protein interactions were examined using PLIP server. As a result, the aptamer AptNR88 with MFE = −41.78 kcal/mol, QGRS score = 62, and GC content = 60.7, as well as the best docking scores and binding interactions, was selected. Binding to the glycoprotein gD

was experimentally confirmed using a colorimetric system with gold nanoparticles (particle sizes 30 nm), which showed a strong correlation between bioinformatics predictions and experimental validation. To our knowledge, this is first study describing a G-quadruplex aptamer for the detection of HSV-1 and HSV-2 in a colorimetric assay.

Materials and methods

In silico design, optimization and selection of G-quadruplex SsDNA aptamers

HSV-1 and HSV-2 glycoprotein gD data preparation

HSV-1 and HSV-2 glycoprotein gD were selected as the most suitable options for the aptamer binding regions. For this purpose, the reported glycoprotein gD sequences of several strains of both HSV-1 and HSV-2 were fetched from NCBI database (https://www.ncbi.nlm.nih.gov). Then, multiple sequence alignments were performed to select the conserved region of the target protein using MultAlin (http://multalin.toulouse.inra.fr). For HSV -1, three crystallographic structures with PDB codes 2C36, 2C3A, and 3U82, and for HSV-2, three structures with PDB codes 4MYV, 3W9E, and 4MYW have been reported. Among the above structures, codes 2C36, 4MYV, and 3W9E were fetched from RCSB PDB database (http://rcsb.org) based on their crystal structure resolution (2.11 Å, 1.8 Å, and 2.30 Å, respectively) and determination under pH conditions similar to clinical samples (6–8).

The structural files were processed using Discovery Studio 2024 Client v.24.1.0 software, to prevent interference in the molecular docking process, duplicate atoms, ligands, and water molecules present in the structural file were removed, and polar hydrogens were added. Energy optimization was performed using YASARA Energy Minimization (https://www.yasara.org/minimizationserver.htm) to optimize atomic positions and enhance structural realism. To evaluate the quality of the final protein files, MolProbity (http://molprobity.biochem.duke.edu) was used. To validate the specific binding of the designed aptamer, human serum albumin (HSA) was chosen as the control protein in the molecular docking studies. HSA, one of the most abundant proteins in human serum and body secretions, was selected to assess the designed aptamer's specificity. Subsequently, aptamers with lower affinity for this protein and higher affinity for gD were selected in the final design stages. The structural file of the HSA protein with PDB code 1AO6 was extracted. Steps of structure preparation were applied, similar to what was performed for gD.

G-quadruplex SsRNA library preparation

A library consisting of 300 random sequences of ssRNA with lengths of 28–36 nucleotides was created. The RNA sequences included four repeats of binary, ternary, and quadruplet G bases and loops with 3–4 random bases. In the next step, the likelihood of forming G-quadruplex structures in the sequences of the ssRNA library was examined using QGRS Mapper (https://bioinformatics.ramapo.edu/QGRS/index.php), and sequences with a score higher than 60 were selected for subsequent structural analysis.

G-quadruplex SsRNA secondary structure prediction

In the past, multiple algorithms have been designed to predict secondary and tertiary structures of oligonucleotides from their sequences. Among several methods for predicting the secondary structure of RNA and DNA, RNAfold algorithms are widely used for secondary structure prediction and can accurately model G-quadruplex formation [28]. The secondary structure of the sequences selected in the previous step was predicted using RNAfold (http://rna.tbi.univie.ac.at//cgi-bin/RNAWebSuite/RNAfold.cgi) The input data consists of a single sequence in text format. The options "RNA parameters" and "incorporate G-quadruplex formation into the structure prediction" algorithms were selected in the Fold algorithms settings. Additionally, the temperature was set to 25 °C in the energy parameters settings.

G-quadruplex SsRNA tertiary structure prediction

Traditionally, experimental methods such as X-ray crystallography, nuclear magnetic resonance (NMR) spectroscopy, and scanning electron microscopy (SEM) have been primarily used to determine the three-dimensional structures of RNA. However, these methods are particularly time-consuming and labor-intensive for RNAs with long sequences or complex structures [29, 30].

Computational modeling of the tertiary structure of RNA and DNA molecules is one of the challenging topics, especially for G-quadruplex structures with non-Watson-Crick hydrogen bonds [31]. In this study, Rosetta FARFAR (RNA De Novo) (https://rosie.rosettacommons.org/rna_denovo) was used. It is important to note that this server only accepts RNA sequences as input. At the time of this study, no powerful alternative tools for predicting the tertiary structure of DNA-specific G-quadruplexes were found. Each ssRNA sequence was submitted to the server. In the next step, the obtained 3D structures were converted from RNA to DNA using the Discovery Studio 2024 Client v.24.1.0 software. Finally, energy optimization was performed on the DNA sequences through the YASARA Energy Minimization.

Molecular docking of SsDNA aptamers with glycoprotein gD

Molecular docking is widely used to predict optimal binding sites between proteins and ligands [32]. In this study, HDOCK (http://hdock.phys.hust.edu.cn) and

HADDOCK 2.4 (https://rascar.science.uu.nl/haddock2.4) were used to investigate the binding of potential DNA aptamers to the glycoprotein gD. To perform molecular docking, previously prepared structural files of the protein and oligonucleotides were uploaded as "receptor" and "ligand" inputs to the server. Subsequently, the results of the molecular dockings were sorted based on the docking scores. The complexes with high docking scores in both docking servers were analyzed in the 2D diagram by PLIP (https://plip-tool.biotec.tu-dresden.de/plip-web/plip/index) to analyze amino acid-nucleotide interactions in protein-DNA complexes [33]. Accordingly, the aptamer binding to the target amino acid region was selected based on its score, number, type of bonds, and binding site. Additionally, their binding scores to the HSA were examined as a negative control for molecular docking. Finally, the aptamer that showed a higher affinity for gD and a lower affinity for HSA was selected.

Experimental studies

Reagents, Materials, and equipment

The designed aptamer was synthesized by TAG Copenhagen (Denmark). Chloroauric acid ($HAuCl_4.3H_2O$) was obtained from Sigma-Aldrich (United States). Hydrochloric acid, nitric acid, methanol, ethanol, potassium chloride (KCl), and trisodium citrate were purchased from Merck Company (Germany). UV/Vis spectrophotometer (Agilent 8453, Agilent Technologies Inc., United States), Particle size analyzer (VASCO, Cordouan Technologies, France), Zeta potential analyzer (SZ-100, Horiba Scientific, Japan), and Fourier transform infrared Spectrometer (Jasco-6300, Japan).

Sample preparation

HSV-infected and control (negative) samples with determined HSV types and cycle threshold (C_T) values were collected from two diagnostic laboratories in Isfahan, Iran. They underwent real-time PCR testing before delivery, and also provided the C_T values and viral load of standard samples for each type. All laboratory procedures for this study were approved by the Biomedical Research Ethics Committee, University of Isfahan, Isfahan, Iran (IR.UI.REC.1402.150). All samples were de-identified and used anonymously, and verbal consent was obtained from the participants. A total of 150 unidentified clinical samples were utilized in this study, all obtained from the cervical fluids of female patients. These included 50 HSV-1-infected samples, 50 HSV-2-infected samples, along with 30 negative samples, 10 VZV-infected samples, and 10 CMV-infected samples. The study's primary objective was the detection of HSV-1 and 2, focusing on the sensitivity and specificity of the developed method; therefore, patient age and weight were not considered as variables. No samples were excluded during the study.

Synthesis and characterization of gold nanoparticles

Gold nanoparticles (AuNPs) were synthesized based on the Turkevich method by reducing chloroauric acid with a trisodium citrate solution [34, 35]. To synthesize nanoparticles, 37.5 µL of 0.1 molar $HAuCl_4$ solution was added to 9 mL of boiling distilled water in an Erlenmeyer flask on a hot plate. In the next step, 1 mL of 2% trisodium citrate solution was quickly added as a reducing and stabilizing agent. Then, the solution was stirred vigorously using a magnetic stirrer at the same temperature for 20 min until the color changed from light yellow to red. To confirm the formation of gold nanoparticles, their absorbance within the 400–700 nm wavelength range was measured using a UV-vis spectrophotometer. Finally, the nanoparticles were characterized by dynamic light scattering (DLS) and zeta potential with a Zetasizer.

Salt tolerance test of AuNPs

The lowest concentration of KCl that induces aggregation of AuNPs, resulting in a color change from red to purple, was determined by testing different KCl concentrations. To perform this test, 10 µL of 200, 300, 400, 450, 500, 600, and 800 mM KCl solutions were added to 200 µL of Au-NPs solution. The color change of the solutions was observed visually after 10 min and analyzed with a UV-vis spectrophotometer. Finally, the lowest effective concentration was selected as the desired concentration for further experiments [36, 37].

Optimization of aptamer concentration

To determine the minimum concentration of aptamer that can prevent aggregation of Au-NPs, 10 µL of 100, 200, 400, and 800 nM and 1, 1.2, and 1.4 µM aptamer solutions were added to 200 µL of Au-NPs solution, and after 30 min, 10 µL of KCl solution with the selected concentration from the previous stage was added. The color change of the Au-NPs was observed, and the optimal aptamer concentration was selected [36–38].

Characterization of aptamer binding to AuNPs

To verify the conjugating process and aptamer binding to the surface of nanoparticles, the size and surface charge of both uncoated and aptamer-coated Au-NPs were determined with a Zetasizer. Additionally, Fourier-transform infrared spectroscopy (FTIR) analysis was used to investigate the interaction of the aptamer with the Au-NPs.

Calculation of the viral load

The standard curve of C_T values obtained from real-time PCR was plotted to determine the virus copy number of HSV-1 and HSV-2 in clinical viral samples. Then, linear interpolation was used with the C_T values of unknown viral samples to calculate the copy number per mL.

Colorimetric assay to determine the limit of detection and specificity of the aptamer

For this purpose, 10 µL of the optimized aptamer solution from the previous step was added to 200 µL of the Au-NPs solution. After 30 min, 10 µL of samples infected with HSV-1 and HSV-2, with a range of 10^{-1}, 10^{1}, 10^{2}, 10^{3}, 10^{4}, 10^{5}, and 10^{6} viral copies/mL, were separately added. Additionally, five control groups were tested, including (a) gold nanoparticles + 10 µL of distilled water, (b) gold nanoparticles + aptamer (without virus), (c) negative control (healthy), (d) sample infected with varicella-zoster virus, and (e) sample infected with cytomegalovirus. After 5 minutes, 10 µL of KCl solution with the specified concentration from the previous step was added to each sample, and 15 min later, a color change was observed visually. The lowest concentration of virus that caused a color change in the Au-NPs solution was considered as the limit of detection of the aptamer [37, 38]. All laboratory experiments were conducted with a minimum of three replicates, and each experiment was performed with a freshly synthesized batch of gold nanoparticles and a different production batch of aptamer AptNR88 to validate the consistency of the results across multiple batches of reagents.

Results

In silico design, optimization and selection of G-quadruplex SsDNA aptamers

HSV-1 and HSV-2 glycoprotein gD data preparation

Glycoprotein gD of herpes simplex viruses generally does not have distinct domains but can be considered based on its three-dimensional structure, which includes three domains: (a) The extracellular domain (residues 26–339 for HSV-1; 26–340 for HSV-2). (b) The transmembrane helical domain (residues 340–361 for both HSV-1 and HSV-2). (c) The intracellular domain (residues 362–394 for HSV-1; 364–393 for HSV-2). These results were derived from data available on UniProt (https://www.uniprot.org). Furthermore, based on the results of MultAlin and considering three important parameters: (a) the most exposed and accessible part of the protein, (b) non-glycosylated regions, (c) the most conserved amino acids, a 95 amino acid segment (residues 162–257, according to the protein sequence file) was identified as the optimal aptamer-binding regions on glycoprotein gD.

Energy optimization of glycoprotein gD structure with codes 4MYV, 2C36, 3W9E, and 1AO6 using the YASARA Energy Minimization indicated that the proteins achieved a more stable, lower energy state after optimization. This structural refinement plays a significant role in the molecular docking process. Following optimization, the structures were saved in PDB format for subsequent analyses. The results obtained from the MolProbity provide information from the Ramachandran plot, including parameters such as the number of residues in favored and allowed regions. Both parameters showed improvement in the 3D structure after energy optimization compared to the initial structure.

G-quadruplex SsRNA library design and structure prediction

First, the G-quadruplex ssRNA library was limited to 120 sequences with scores above 60 based on QGRS Mapper. In the next step, the minimum free energy (MFE) of the ssRNA secondary structures was analyzed using RNAfold as an indicator of stability. RNAfold can predict the formation of G-quadruplexes and represents the G-tetrad interactions with dashed lines in secondary structure diagrams, it does not differentiate between specific topologies such as parallel, antiparallel, or hybrid folds. The MFE values presented in Table 1 reflect the overall thermodynamic stability of these predicted secondary structures. 40 ssRNA sequences with MFE values lower than −40 kcal/mol were selected for tertiary structure prediction. The top 10 sequences based on their

Table 1 The top 10 sequences, identified based on QGRS score, GC content, and minimum free energy, were ranked according to their minimum free energy values

Aptamer	Sequence	Minimum free energy (kcal/mol)	QGRS score	GC content (%)
AptNR55	GTCAGGGGTGGGGAGGGGTGGGGTGAC	−70.41	63	74
AptNR66	GCAAGGGGTGGGGTGGGGAGGGGTTGC	−69.86	63	74
AptNR99	ATATGGGGTGGGGAGGGGTGGGG	−65.76	63	69.5
AptNR44	CGGTGGGGAGGGGTAGGGGACGGGGACCG	−58.81	62	79.3
AptNR11	TGTGGGGAAAGGGGAGGGGCGGGGACA	−54.21	61	70.3
AptNR33	GGCAGGGGTAGGGGACGGGGTGAGGGGTGCC	−54.05	62	77.4
AptNR22	TAGTGGGGCAGGGGTAGGGGTAGGGGACTA	−52.43	63	63.3
AptNR10	TCAGGGGTGTGGGGATGGGGTCGAGGGGTAT	−43.32	61	64.5
AptNR111	GGGGTCTGGGGAAAGGGGTTAGGGGCCTGGGG	−43.32	63	71.8
AptNR77	GGGGAGTGGGGACAGGGGAACGGGGTAA	−43.32	63	67.8
AptNR88	**GGGGTATAGGGGACTGGGGTAAGGGGAT**	**−41.78**	**62**	**60.7**

AptNR88 was the selected aptamer for further analysis in the study

QGRS scores, MFE values, and GC content percentages are shown in Table 1. The secondary structures of five of them with the highest molecular docking scores, predicted by RNAfold, are shown in Fig. 1. The tertiary structure of all 40 sequences selected based on the previous screening criteria, including the selected aptamer AptNR88 (all sequences were ssRNA), was obtained by Rosetta FARFAR and subsequently modified, including conversion of uracil to thymine (RNA-to-DNA conversion) and energy optimization. The tertiary structures of AptNR88 in complex with glycoprotein gD are shown in Fig. 2.

Molecular docking of SsDNA aptamers with glycoprotein gD

Molecular docking of the 40 sequences selected in the previous stages with glycoprotein gD was performed to investigate their binding affinities and interaction regions using HDOCK and HADDOCK. The five ssRNA sequences with the best molecular docking scores are shown in Table 2. Selection of AptNR88 was made based on a comprehensive evaluation of multiple quantitative criteria. First, as shown in Table 2, AptNR88 exhibited the highest binding score for all three glycoprotein gD structures (2C36, 4MYV, and 3W9E) on both HDOCK and HADDOCK servers. Specifically, it showed docking scores of −303.4, −311 and − 285.2 for, respectively, 2C36, 4MYV and 3W9E, with HDOCK, and of −110, −114 and − 92 for, respectively, 2C36, 4MYV and 3W9E with HADDOCK. These scores were significantly more favorable than those of the other top candidates. Additionally, aptamer AptNR88 showed the lowest binding affinity for the negative control protein (HSA) with scores of −220 (HDOCK) and − 50 (HADDOCK). The interaction regions of the AptNR88 and glycoprotein gD are shown in Fig. 2. Another factor taken into consideration was the analysis of the binding interactions.

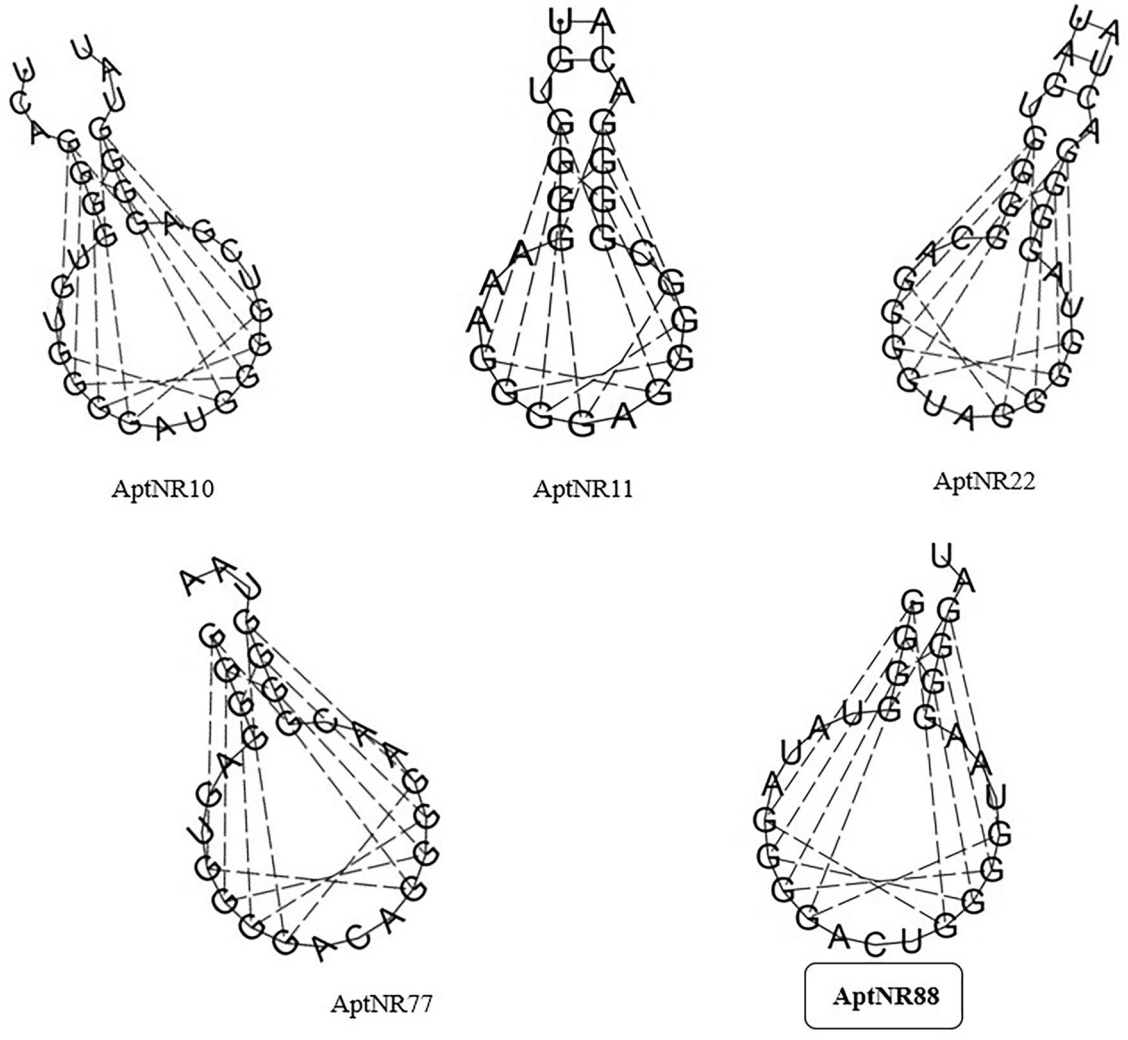

Fig. 1 The secondary structures of the five ssRNA sequences with the highest docking scores were predicted by RNAfold. AptNR88 was selected as the aptamer for further analysis in the study. Dashed lines show G-G interactions responsible for the formation of the G-quadruplex structure

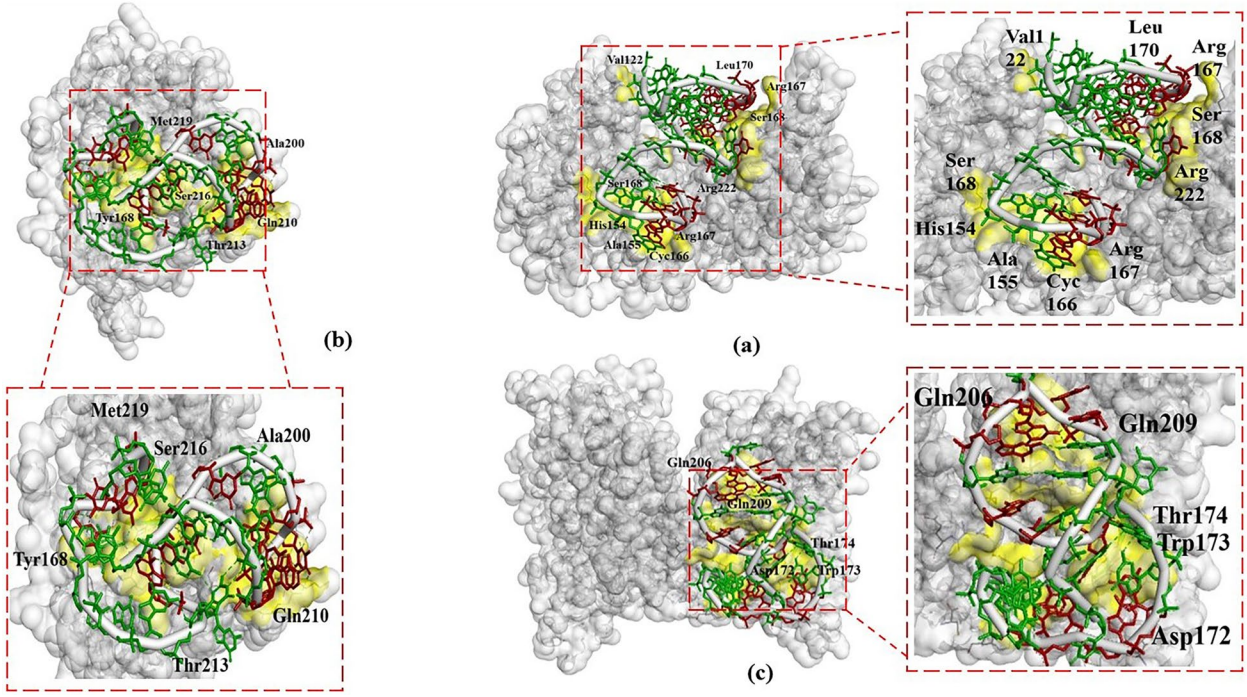

Fig. 2 The interaction regions of AptNR88 with three structural models, 4MYV (**a**), 3W9E (**b**), 2C36 (**c**), have been shown using the Discovery Studio program. Hydrogen bonding regions are highlighted in yellow, and the involved amino acids are shown

Table 2 Molecular docking scores of the top five aptamers obtained from HDOCK and HADDOCK

Aptamer	HDOCK				HADDOCK			
	2C36	4MYV	3W9E	1AO6	2C36	4MYV	3W9E	1AO6
AptNR10	−277	−260	−253.8	−231	−95	−92	−75	−60
AptNR22	−281	−269	−271	−239	−102	−68	−92	−58
AptNR77	−260	−250.2	−268	−230	−92	−58	−102	−58
AptNR88	−303.4	−311	−285.2	−220	−110	−114	−92	−50
AptNR11	−261	−250	−245	−221	−95	−58	−55	−45

Table 3 Interaction data between AptNR88 and the glycoprotein gD were obtained from PLIP

gD PDB file	Interaction				
	Hydrogen bonds	Hydrophobic interactions	π-Stacking interactions	π-Cation interactions	Salt bridge
2C36	15	4	–	2	1
3W9E	9	2	–	–	3
4MYV	12	2	1	2	4

Several hydrogen bonds, hydrophobic interactions, and other types of interactions were identified between AptNR88 and the glycoprotein gD. The counts for each type of interaction analyzed by PLIP are detailed in Table 3. AptNR88 formed a greater number of hydrogen bonds and electrostatic interactions with glycoprotein gD compared to the other aptamers. For example, it formed 15, 9 and 12 hydrogen bonds with, respectively, 2C36, 3W9E and 4MYV with 12 hydrogen bonds. Specific interactions, including the amino acids and nucleotides involved, are carefully described in Table 4, which further confirms the strong binding characteristics of aptamer AptNR88 to the target protein region.

Experimental studies

Synthesis and characterization of AuNPs

AuNPs were synthesized by reducing $HAuCl_4$ with trisodium citrate. UV-vis spectroscopy showed a strong absorption peak at 520 nm with an absorbance of 0.521 (Fig. 3), indicating an appropriate particle size of approximately 30 nm, as also confirmed by DLS measurements (Fig. S1a). Additionally, a pH of 6.1 was measured for the synthesized AuNPs. According to studies, AuNPs with a size in the range 10–50 nm show a maximum absorption peak between 520 and 530 nm, and with the increase in size, a gradual red shift toward longer wavelengths is observed [39]. The analysis indicated that the surface of the AuNPs was covered adequately with negatively charged citrate groups (−14.33 mV; Fig. S2a), leading to stability of the AuNP colloid.

Table 4 Amino acids and nucleotides involved in interactions between AptNR88 and glycoprotein gD (residues 162–257)

gD PDB file	4MYV		3W9E		2C36	
Interaction	**Nucleotide**	**Amino acid**	**Nucleotide**	**Amino acid**	**Nucleotide**	**Amino acid**
Hydrogenic	DT20	Glu159A	DA21	Ala200A	DT7, DG9	Asp172B
	DG12, DG23	Glu182A	DT20 (×2)	Gln210A	DA8	Trp173B
	DA22	His183A	DA21	Thr213A	DA13	Thr174B
	DG12	Arg184A	DA22 (×2)	Ser216A	DG19	Gln206B
	DA8	Glu159B	DT15	Met219A	DG19, DA21	Gln209B
	DA8 (×2)	Glu182B				
	DG9	His183B				
	DG9	Arg184B				
Hydrophobic	DA22	His183A	DT20	Ala207A	DA13	Asp172B
			DT15	Asp215A		
Salt bridge	DG12	Glu182A	DG4	Arg222A	DC14	Lys169B
	DG23,24	Arg184A				

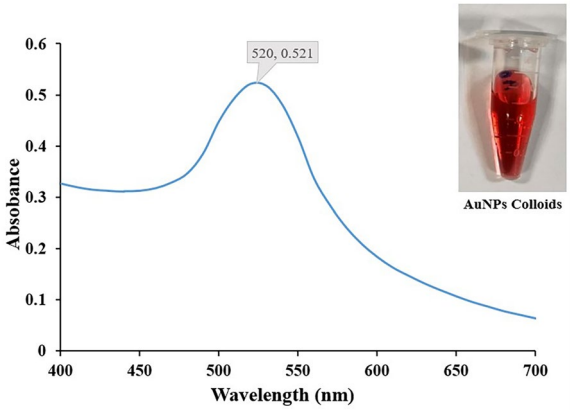

Fig. 3 Absorbance spectrum of the synthesized gold nanoparticles in the 400–700 nm wavelength range

Salt tolerance test of AuNPs and optimization of aptamer concentration

In the salt-induced aggregation test, KCl concentrations in the range 200–800 mM were used. The AuNP colloid showed resistance at a concentration of 200 mM but became increasingly sensitive at concentrations of 300 mM or higher. Salt-induced aggregation of nanoparticles caused a red shift of the absorption peak and a visible color change to purple. It is important to note that a visible color change can be observed at lower concentrations (e.g., 300 mM) due to the initial stages of aggregation, even before a major red shift in the absorption peak. Based on the results, a concentration of 300 mM KCl was selected as the lowest concentration that caused a color change of the nanoparticles from red to purple within the specified time of 10 min (Figs. 4a and 5a).

At the selected KCl amount, the optimal aptamer concentration, which prevented the aggregation of AuNPs and caused a color change to purple, was determined to be 1 µM, with 10 µL added (Figs. 4b and 5b). The selection of 1 µM as the optimal aptamer concentration was based on the highest stability against salt-induced aggregation, peak intensity and symmetry, aptamer over-saturation that caused non-specific aggregation of AuNPs. At this concentration, DNA aptamers are adsorbed on the AuNP surface through interactions involving the nitrogen atoms, N3 and N7 sites, of adenine and guanine bases [40]. These interactions are strong and can overcome the electrostatic repulsion between the phosphate backbone and AuNPs, both negatively charged [41]. As a result, the negatively charged groups of the DNA aptamers are exposed to the surface and induce electrostatic repulsion between AuNPs [42, 43].

Characterization of aptamer binding to AuNPs

DLS tests indicated that the average hydrodynamic radius of AuNPs was 29.54 nm, whereas the aptamer-coated AuNPs had measured 38.94 nm (Fig. S1b). The zeta potential of the aptamer-coated AuNPs was – 25.03 mV, while for the AuNPs it was – 14.33 mV (Fig. S2b). The FTIR spectra of uncoated and aptamer-coated AuNPs (Fig. S3) indicated that aptamer coating increases light transmittance, which means reduced light absorption. This may result from surface coverage by aptamers and changes in the electronic environment. There is a peak near 3425.92 cm^{-1} in both AuNPs and aptamer-coated AuNPs. A decrease in the intensity of this band indicates hydrogen bond formation (strong dipole-dipole interaction) and an effect on N-H stretching vibrations, suggesting aptamer binding through amine groups. The 1583.27 cm^{-1} peak (aromatic C = C vibrations) and 1397.17 cm^{-1} peak (O-H bending and carboxylic groups of the aptamer showed a clear presence in the coated sample) show decreased intensity upon coating, supporting aptamer adsorption. Similarly, the reduced intensity at 624.32 cm^{-1} (Au-O or Au-N bonds) implies fewer active metal bonds due to surface coverage. These spectral changes confirm aptamer-nanoparticle interactions modifying vibrational characteristics and leading to reduced absorption at specific wavelengths.

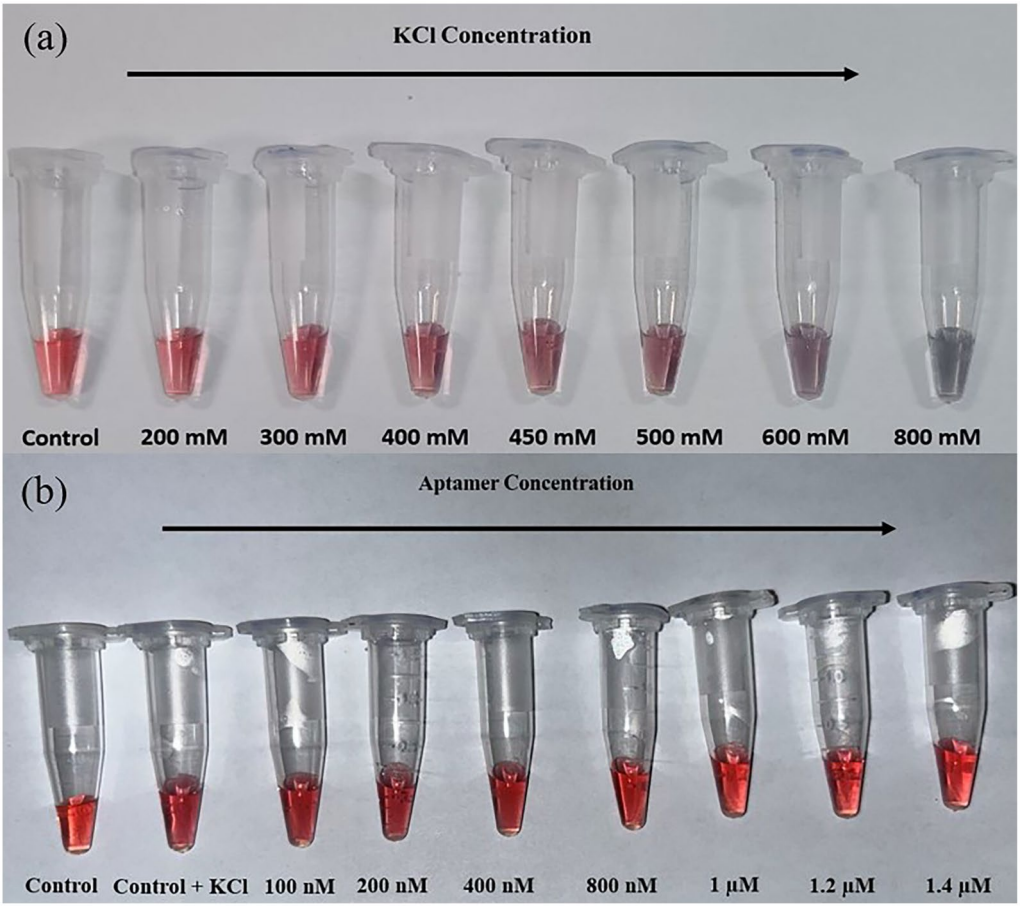

Fig. 4 (**a**) Salt tolerance test of AuNPs in the presence of KCl at concentrations in the range 200–800 mM, measured 10 min after KCl addition. **b** Optimization of aptamer concentration from 100 nM to 1.4 µM, performed in the presence of 300 mM KCl and measured after 10 min

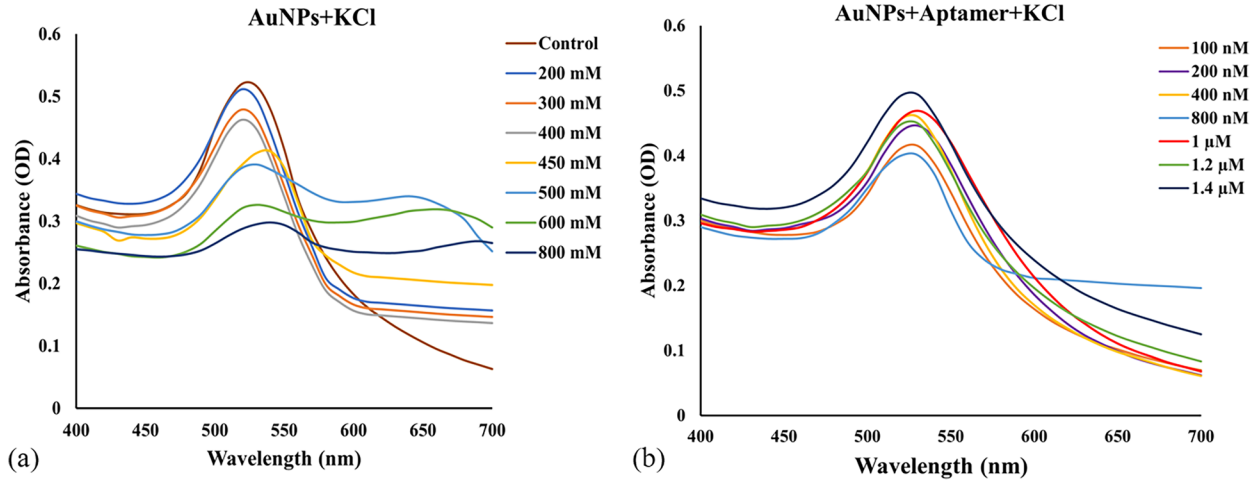

Fig. 5 UV-vis absorbance spectra of AuNPs measured in the 400–700 nm wavelength range: (**a**) in the presence of KCl concentrations ranging from 200 mM to 800 mM, and (**b**) in the presence of aptamer concentrations from 100 nM to 1.4 µM at a fixed KCl concentration of 300 mM

Calculation of the viral load

After plotting a standard curve of cycle threshold (C_T) values using linear interpolation, the viral copy number per mL was calculated for each sample. The virus copy number of the viral samples was determined by applying the standard curve to serially diluted samples. The graph of C_T values (Fig. 6) was linear and showed an acceptable correlation for HSV-1 ($R^2 = \sim 0.98$) and HSV-2

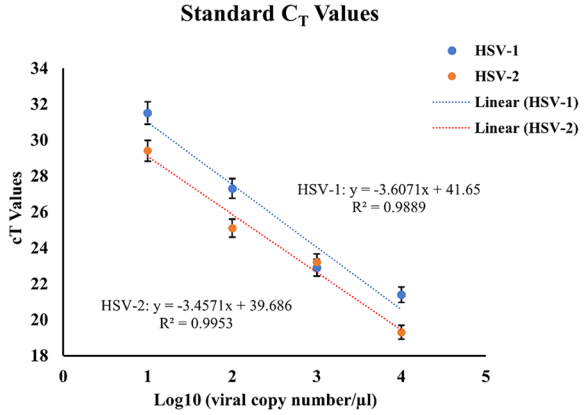

Fig. 6 Standard curve of C_T values for detecting HSV-1 and HSV-2

($R^2 = \sim 0.99$). The results indicate HSV-1 copy numbers ranged from 1.17×10^1 to 1.52×10^6 copies/mL, while HSV-2 ranged from 1.57×10^1 to 6×10^5 copies/mL in viral samples.

Colorimetric assay to determine the limit of detection and specificity of the aptamer

The limit of detection and specificity of the aptamer-AuNPs sensor for HSV-1 and HSV-2 were investigated. As shown in Fig. 7, the addition of 10 µL of 300 mM KCl into the vials containing viral concentrations ranging from $1.17 \cdot 10^1$ to $1.52 \cdot 10^6$ copies/mL for HSV-1 and from $1.57 \cdot 10^1$ to $6 \cdot 10^5$ copies/mL for HSV-2 induced aggregation of the AuNPs and caused the color change from red to purple. In contrast, no color change was observed in the aptamer-coated AuNPs, the aptamer-coated AuNPs + negative control, and the aptamer-coated AuNPs + VZV and CMV after KCl addition. Based on the results shown in Fig. 7, the designed aptamer-AuNPs sensor can detect HSV-1 and HSV-2 at low virus concentrations, specifically $1.17 \cdot 10^1$ copies/mL for HSV-1 and $1.57 \cdot 10^1$ copies/mL for HSV-2.

Discussion

Today, the application of in silico methods has significantly transformed biological research by enabling valuable predictive insights, and this field continues to evolve with the advent of advanced computational tools such as machine learning and artificial intelligence. Additionally, in silico studies using bioinformatics tools, including databases, online and offline servers, and specialized software, have become one of the favored fields for the design and optimization of aptamers. These studies utilize bioinformatics methods to design novel aptamers or to refine those obtained via SELEX. Since the onset of the COVID-19 pandemic, researchers have increasingly employed bioinformatics approaches to develop effective prevention and treatment strategies. Studies have demonstrated that bioinformatics methods, including molecular docking, apply to modeling interactions between oligonucleotides and proteins. These insights support the use of antiviral aptamers as a promising strategy for virus detection and treatment.

In literatures, aptamers for targeting HSV were studied for antiviral effects rather than diagnostics. Gopinath et al. similarly evolved an RNA aptamer against HSV-1 gD with an IC_{50} = 0.8 µM, specific enough to distinguish HSV-1 from HSV-2 [43]. Yadavalli et al. identified a 45-nt DNA aptamer binding glycoprotein D with Kd = 50 nM, significantly blocking viral entry in vitro and in vivo for HSV-1 [44]. In our previous study, we developed an aptasensor for the rapid detection of white spot syndrome virus in shrimp [41]. We used an aptamer-functionalized AuNP-based colorimetric technique and achieved a limit of detection (LOD) of 10^4 copies. In addition, the aptamer used in our work was designed using bioinformatics tools. Lerga et al. used an aptamer-AuNP system similar to the system described in our study for the determination of histamine in food products [45]. Their biosensor showed a good correlation with the results of HPLC and ELISA kits as standard methods for measuring histamine. D.R. Martin et al. used in silico methods such as Phyre2, RNAfold, RNAComposer, HADDOCK, and GROMACS to model the structures of the Ebola virus NP protein and its aptamer candidates. After selecting the aptamers using the SELEX method, they studied the binding interactions between the aptamers and the target protein. These analyses showed that all three aptamers successfully bound to the target protein [46]. Michael D. Schump et al. developed neutralizing DNA aptamers targeting HSV-1 and HSV-2. The aptamers were selected against glycoprotein gD from both viruses in parallel via the SELEX method. The aptamers were tested in a guinea pig model of HSV-2 vaginal infection, where they significantly reduced both viral load and disease severity. These results demonstrate that the designed aptamers were effective against HSV-1 and HSV-2 [47].

In this study, in addition to evaluating the credibility and limitations of each bioinformatics tool, their citation frequency was also considered to identify the most appropriate tools. While the final aptamer is a DNA molecule, tools developed for RNA, such as RNAfold and Rosetta FARFAR, were initially used. This decision stems from the superior algorithms and higher reliability of these tools for predicting G-quadruplex structures, a feature often not found with this accuracy in DNA prediction tools. For example, since the goal was to design a G-quadruplex-forming aptamer, RNAfold was selected among several reputable secondary structure prediction servers (e.g., UNAFold, ViennaRNA, MFold) due to its specific capabilities. This server supports the prediction of quadruplex structures and offers superior performance in predicting complex structures compared to alternative

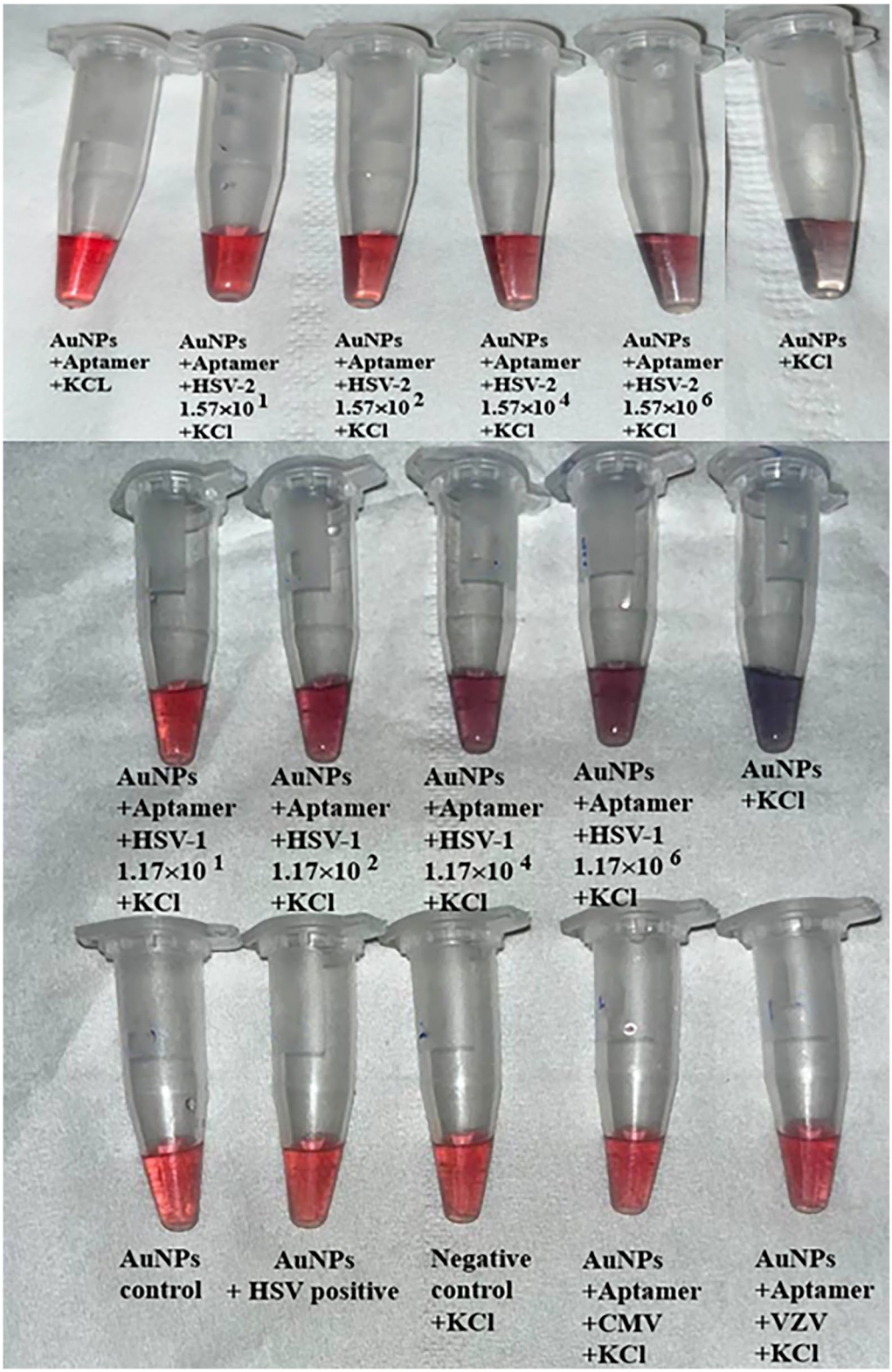

Fig. 7 Color change of AuNPs from red to purple in the presence of aptamer, KCl, and varying concentrations of viral target. For HSV-1, concentrations ranged from 1.17×10^{1} to 1.52×10^{6} copies/mL, and for HSV-2, from 1.57×10^{1} to 6×10^{5} copies/mL. Negative controls: aptamer-coated AuNPs, HSV-negative samples, and viral samples of VZV and CMV. Positive control: unmodified AuNPs

tools. An additional advantage is the ability to set the prediction temperature, which allows structure determination at 25 °C, matching the room-temperature conditions used in experimental testing. To predict the tertiary structure of aptamers, Rosetta FARFAR was selected over alternatives such as RNAComposer, Vfold3D, and UNAFold due to its support for modeling G-quadruplex formations. However, one of the limitations of this server is its inability to process RNA sequences longer than 32 nucleotides. This limitation led to considering a positive feature for the short length of the aptamer sequence; consequently, the sequences of the aptamer library were determined to be between 28 and 32 nucleotides. Tools for predicting G-quadruplex DNA, such as QGRS-quadruplex and G4-iM Grinder, are often limited to sequence-based predictions and may not be as capable of predicting complete tertiary structures or incorporating complex folding parameters as Rosetta FARFAR.

Various tools are available for molecular docking studies, including ZDOCK, NPDOCK, ClusPro, AutoDock Vina, and RosettaDock. HDOCK and HADDOCK were selected for their advanced capabilities in modeling protein-nucleic acid interactions. Most molecular docking tools are limited to protein-ligand or protein-protein interactions, whereas only a few are developed for protein-peptide or protein-nucleic acid complexes. They utilize hybrid algorithms combining template-based and ab initio docking methods to predict molecular interactions. Furthermore, these servers accept amino acid sequences as input and incorporate experimental data, such as protein-binding site information and small-angle X-ray scattering, into a hybrid docking strategy. Using two different docking servers provided a cross-validation approach; only aptamers that performed well in both were selected.

During the analysis of aptamer–protein interactions, PLIP was selected for its strong interaction profiling, clear differentiation of bond types, and detailed reporting of bond counts and characteristics. This server can characterize hydrogen bonds, electrostatic and hydrophobic interactions, π-π stacking, salt bridges, van der Waals forces, or combinations thereof within the complex. Hydrogen bonding is reported to be the most prevalent interaction between aptamers and their target molecules. Therefore, the presence and number of hydrogen bonds were considered key screening parameters for identifying the aptamer with the most favorable binding characteristics. Ultimately, AptNR88 was selected based on the comprehensive evaluation and limitations. Notably, AptNR88 achieved the highest docking scores with all three structural models of glycoprotein gD from HSV-1 and HSV-2, primarily due to strong electrostatic interactions. In contrast, it showed the lowest docking scores with the HSA on both servers, indicating target specificity. It is also known that while our in silico predictions strongly indicate the G-quadruplex structure, comprehensive structural characterization using experimental methods such as circular dichroism (CD) spectroscopy and UV melting analysis was beyond the scope of this study. This remains a crucial next step to fully validate the predicted structure. However, the functional success of aptamers in colorimetric measurements provides strong experimental evidence of their ability to bind to the target protein.

HSV detection in diagnostic and research laboratories is performed using various methods. The most widely used methods include real-time PCR and ELISA, which are based on the detection of the viral genome or the detection of the antigen-antibody. Although most current methods are highly accurate, they rely heavily on antibodies. Compared to antibodies, aptamers are smaller, more thermostable, less costly to produce, and easily modifiable. Therefore, aptamers hold strong potential for use in the development of cost-effective diagnostic tests. Moreover, since common diagnostic tests such as real-time PCR and ELISA must be performed in a laboratory, these tests cannot be used at the point of care (POC) because samples must first be transported to a laboratory, require trained personnel, are costly, and need a significant volume of samples. Therefore, development of new diagnostic techniques that are accurate and rapid is essential for the next generation of diagnostic technology.

Conclusion

In this study, bioinformatics tools were used to design a de novo G-quadruplex aptamer, and a colorimetric biosensor based on G-quadruplex-functionalized AuNPs for the detection of HSV-1 and HSV-2 was successfully developed. This biosensor achieved a low detection limit of $1.17 \cdot 10^1$ copies/mL for HSV-1 and $1.57 \cdot 10^1$ copies/mL for HSV-2. In addition, the biosensor offers advantages such as simplicity, speed, naked-eye detectability, and low cost that can make our developed biosensor a suitable candidate for a rapid detection method. The aptamer used as the recognition element was designed in silico. The specific binding of the G-quadruplex aptamer to HSV-1 and HSV-2 was experimentally confirmed. Validation experiments indicated superior performance compared to standard methods such as real-time PCR and ELISA. The designed G-quadruplex aptamer demonstrated high selectivity and sensitivity for both viruses, emphasizing the potential of bioinformatics techniques in aptamer selection.

Supplementary Information

The online version contains supplementary material available at https://doi.org/10.1186/s12985-025-02949-7.

Supplementary Material 1.

Acknowledgements
Support for this work by the University of Isfahan is highly acknowledged.

Author contributions
Sepehr Nouri (S.N.): Contributed to the conceptualization of the study, performed the in silico aptamer design, conducted the experimental investigations, collected data, prepared all figures, tables, and supplementary materials, was responsible for data analysis and interpretation, wrote the original draft of the manuscript, and reviewed and edited the manuscript. Soheil Shajari (S.S.): Contributed to the conceptualization of the study, performed the in silico aptamer design, conducted the experimental investigations, collected data, prepared all figures, tables, and supplementary materials, wrote the original draft of the manuscript, and reviewed and edited the manuscript.Hassan Mohabatkar (H.M.): Contributed to data curation and formal analysis, supervised the in silico aptamer design, provided overall supervision for the project, and reviewed and edited the manuscript.Mandana Behbahani (M.B.): Contributed to data curation and formal analysis, supervised the in silico aptamer design, and reviewed and edited the manuscript.All authors read and approved the final manuscript.

Funding
The author(s) received no specific funding for this work.

Data availability
The data that support the findings of this study are available within the article and its supporting information files.

Declarations

Ethics approval and consent to participate
All laboratory procedures for this study were approved by the Biomedical Research Ethics Committee, University of Isfahan, Isfahan, Iran (Ethics committee reference number: IR.UI.REC.1402.150). All methods were performed under the relevant guidelines and regulations. The project was found to be under the ethical principles of the Declaration of Helsinki and the national norms and standards for conducting Medical Research in Iran.

Consent for publication
Not applicable.

Competing interests
The authors declare no competing interests.

Author details
[1]Department of Biotechnology, Faculty of Biological Science and Technology, University of Isfahan, Isfahan, Iran

Received: 22 July 2025 / Accepted: 17 September 2025
Published online: 27 October 2025

References

1. Whitley RJ. Herpesviruses. In: Baron S, editor. Medical microbiology. Galveston (TX): University of Texas Medical Branch at Galveston; 1996. p. 1–24.
2. Ryan KJ, Ray CG, Sherris JC. Sherris Medical Microbiology. 2010.
3. Chayavichitsilp P, Buckwalter JV, Krakowski AC, Friedlander SF. Herpes simplex. Pediatr Rev. 2009;30(4):119–30.
4. Fleming DT, McQuillan GM, Johnson RE, Nahmias AJ, Aral SO, Lee FK, et al. Herpes simplex virus type 2 in the United States, 1976 to 1994. N Engl J Med. 1997;337(16):1105–11.
5. Corey L, Spear PG. Infections with herpes simplex viruses. N Engl J Med. 1986;314(11):686–91.
6. Organization WH, Herpes Simplex V. 2023. Available from: https://www.who.int/news-room/fact-sheets/detail/herpes-simplex-virus
7. McGeoch DJ, Rixon FJ, Davison AJ. Topics in herpesvirus genomics and evolution. Virus Res. 2006;117(1):90–104.
8. Davison AJ. Comparative analysis of the genomes. Human Herpesviruses: Biology, Therapy, and Immunoprophylaxis. 2007.
9. McGEOCH DJ, Moss HW, McNAB D, Frame MC. DNA sequence and genetic content of the Hin dIII I region in the short unique component of the herpes simplex virus type 2 genome: identification of the gene encoding glycoprotein G, and evolutionary comparisons. J Gen Virol. 1987;68(1):19–38.
10. Heming JD, Conway JF, Homa FL. Herpesvirus capsid assembly and DNA packaging. Cell Biology Herpes Viruses. 2017;223:119–42.
11. Das D, Hong J. Herpesvirus polymerase inhibitors. Viral polymerases. 333 – 56; 2019.
12. Liu Y-T, Jih J, Dai X, Bi G-Q, Zhou ZH. Cryo-EM structures of herpes simplex virus type 1 portal vertex and packaged genome. Nature. 2019;570(7760):257–61.
13. Whitbeck JC, Peng C, Lou H, Xu R, Willis SH, Ponce de Leon M, et al. Glycoprotein D of herpes simplex virus (HSV) binds directly to HVEM, a member of the tumor necrosis factor receptor superfamily and a mediator of HSV entry. J Virol. 1997;71(8):6083–93.
14. Bai L, Xu J, Zeng L, Zhang L, Zhou F. A review of HSV pathogenesis, vaccine development, and advanced applications. Mol Biomed. 2024;5(1):1–30.
15. Carfì A, Willis SH, Whitbeck JC, Krummenacher C, Cohen GH, Eisenberg RJ, et al. Herpes simplex virus glycoprotein d bound to the human receptor HveA. Mol Cell. 2001;8(1):169–79.
16. Lu G, Zhang N, Qi J, Li Y, Chen Z, Zheng C, et al. Crystal structure of herpes simplex virus 2 gD bound to nectin-1 reveals a conserved mode of receptor recognition. J Virol. 2014;88(23):13678–88.
17. Hulo C, De Castro E, Masson P, Bougueleret L, Bairoch A, Xenarios I, et al. ViralZone: a knowledge resource to understand virus diversity. Nucleic Acids Res. 2011;39(suppl1):D576–82.
18. Johnston C, Magaret A, Son H, Stern M, Rathbun M, Renner D, et al. Viral shedding 1 year following first-episode genital HSV-1 infection. JAMA. 2022;328(17):1730–9.
19. Sperling RS, Fife KH, Warren TJ, Dix LP, Brennan CA. The effect of daily valacyclovir suppression on herpes simplex virus type 2 viral shedding in HSV-2 seropositive subjects without a history of genital herpes. Sex Transm Dis. 2008;35(3):286–90.
20. Whitley RJ, editor. Herpes simplex virus infection. Seminars in pediatric infectious diseases. 2002.
21. Fatahzadeh M, Schwartz RA. Human herpes simplex virus infections: epidemiology, pathogenesis, symptomatology, diagnosis, and management. J Am Acad Dermatol. 2007;57(5):737–63.
22. Looker KJ, Elmes JA, Gottlieb SL, Schiffer JT, Vickerman P, Turner KM, et al. Effect of HSV-2 infection on subsequent HIV acquisition: an updated systematic review and meta-analysis. Lancet Infect Dis. 2017;17(12):1303–16.
23. LeGoff J, Péré H, Bélec L. Diagnosis of genital herpes simplex virus infection in the clinical laboratory. Virol J. 2014;11:1–17.
24. Farzin L, Shamsipur M, Sheibani S. A review: aptamer-based analytical strategies using the nanomaterials for environmental and human monitoring of toxic heavy metals. Talanta. 2017;174:619–27.
25. Liu M, Xu S, Guo Y, Sun X, Marrazza G. Recent advances in functionally engineered aptamers: strategies and applications. Top Curr Chem. 2025;383(3):1–38.
26. Roxo C, Kotkowiak W, Pasternak A. G-Quadruplex-Forming aptamers-characteristics, applications, and perspectives. Molecules. 2019;24(20):3781.
27. Napolitano E, Criscuolo A, Riccardi C, Esposito CL, Catuogno S, Coppola G, et al. Directing in vitro selection towards G-quadruplex-forming aptamers to inhibit HMGB1 pathological activity. Angew Chem. 2024;136(16):e202319828. https://doi.org/10.1002/ange.202319828
28. Afanasyeva A, Nagao C, Mizuguchi K. Prediction of the secondary structure of short DNA aptamers. Biophys Physicobiol. 2019;16:287–94.
29. Wang X, Yu S, Lou E, Tan Y-L, Tan Z-J. RNA 3D structure prediction: progress and perspective. Molecules. 2023;28(14):5532.
30. Shi Y-Z, Wu Y-Y, Wang F-H, Tan Z-J. RNA structure prediction: progress and perspective. Chin Phys B. 2014;23(7):078701.
31. Yesselman JD, Das R. Modeling small noncanonical RNA motifs with the Rosetta FARFAR server. RNA Structure Determination: Methods and Protocols. 2016:187 – 98.
32. Lee SJ, Cho J, Lee B-H, Hwang D, Park J-W. Design and prediction of aptamers assisted by in Silico methods. Biomedicines. 2023;11(2):356.
33. Salentin S, Schreiber S, Haupt VJ, Adasme MF, Schroeder M. PLIP: fully automated protein–ligand interaction profiler. Nucleic Acids Res. 2015;43(W1):W443-7.
34. Dong J, Carpinone PL, Pyrgiotakis G, Demokritou P, Moudgil BM. Synthesis of precision gold nanoparticles using Turkevich method. KONA Powder Part J. 2020;37:224–32.
35. Rohiman A, Anshori I, Surawijaya A, Idris I, editors. Study of colloidal gold synthesis using Turkevich method. AIP Conference Proceedings. 2011.

36. Bai W, Zhu C, Liu J, Yan M, Yang S, Chen A. Gold nanoparticle–based colorimetric aptasensor for rapid detection of six organophosphorous pesticides. Environ Toxicol Chem. 2015;34(10):2244–9.
37. Zhao W, Brook MA, Li Y. Design of gold nanoparticle-based colorimetric biosensing assays. Chembiochem. 2008;9(15):2363–71.
38. Li X, Cheng R, Shi H, Tang B, Xiao H, Zhao G. A simple highly sensitive and selective aptamer-based colorimetric sensor for environmental toxins microcystin-LR in water samples. J Hazard Mater. 2016;304:474–80.
39. He YQ, Liu SP, Kong L, Liu ZF. A study on the sizes and concentrations of gold nanoparticles by spectra of absorption, resonance Rayleigh scattering and resonance non-linear scattering. Spectrochim Acta A Mol Biomol Spectrosc. 2005;61(13–14):2861–6.
40. Zhang X, Servos MR, Liu J. Surface science of DNA adsorption onto citrate-capped gold nanoparticles. Langmuir. 2012;28(8):3896–902.
41. Etedali P, Behbahani M, Mohabatkar H, Dini G. Field-usable aptamer–gold nanoparticles-based colorimetric sensor for rapid detection of white spot syndrome virus in shrimp. Aquaculture. 2022;548:737628.
42. Farahani N, Behmanesh M, Ranjbar B. A comparative study of DNA loading on the positive and negative surface charge gold nanoparticles. Modares J Biotechnol. 2019;10(3):447–54.
43. Gopinath SC, Hayashi K, Kumar PK. Aptamer that binds to the gD protein of herpes simplex virus 1 and efficiently inhibits viral entry. J Virol. 2012;86(12):6732–44.
44. Yadavalli T, Agelidis A, Jaishankar D, Mangano K, Thakkar N, Penmetcha K, et al. Targeting herpes simplex virus-1 gD by a DNA aptamer can be an effective new strategy to curb viral infection. Mol Ther. 2017;9:365–78.
45. Lerga TM, Skouridou V, Bermudo MC, Bashammakh AS, El-Shahawi MS, Alyoubi AO, et al. Gold nanoparticle aptamer assay for the determination of histamine in foodstuffs. Microchim Acta. 2020;187:1–9.
46. Martin D, Mutombwera A, Madiehe A, Onani M, Meyer M, Cloete R. Molecular modeling and simulation studies of SELEX-derived high-affinity DNA aptamers to the Ebola virus nucleoprotein. J Biomol Struct Dynamics. 2024;43(9):4405-4422.
47. Schump MD, Bernstein DI, Bravo FJ, Neff CP. Selection, activity, and nuclease stabilization of cross-neutralizing DNA aptamers targeting HSV-1 and HSV-2. Virology. 2024;589:109916.

Publisher's note